Environmental Research 212 (2022) 113255

Contents lists available at ScienceDirect

Environmental Research

journal homepage: www.elsevier.com/locate/envres

Chemical composition, sources and optical properties of nitrated aromatic compounds in fine particulate matter during winter foggy days in Nanjing, China

Chenjuan Gu [a], Shijie Cui [a], Xinlei Ge [a,*], Zhiying Wang [a], Meijuan Chen [a], Zihe Qian [a], Zhiyi Liu [b], Xinfeng Wang [b], Yunjiang Zhang [a,**]

[a] Jiangsu Key Laboratory of Atmospheric Environment Monitoring and Pollution Control, Collaborative Innovation Center of Atmospheric Environment and Equipment Technology, School of Environmental Science and Engineering, Nanjing University of Information Science and Technology, Nanjing, 210044, China
[b] Environmental Research Institute, Shandong University, Qingdao, 266237, China

ARTICLE INFO

Keywords:
Nitrated aromatic compounds
Chemical analysis
Sources
Optical properties
Fog

ABSTRACT

Functionalized aromatic compounds are one of the most important light-absorbing organic chromophores – so-called brown carbon (BrC) – in fine particulate matter ($PM_{2.5}$). In this study, we conducted a wintertime field campaign to measure eight nitrated aromatic compounds (NACs) in $PM_{2.5}$ with offline analysis techniques, including liquid chromatograph mass spectrometer (LC-MS) and aerodyne high-resolution aerosol mass spectrometer (AMS) measurements, during foggy and nonfoggy days in suburban Nanjing in the Yangtze River Delta region, China. On average, 4-nitrophenol could be one of the most important light absorbing materials in the observed BrC, which accounted for over 40% of the mass concentration of identified chromophores. The mass concentration of 2-methyl-4-nitrophenol and 2,6-dimethyl-4-nitrophenol were evidently increased during foggy days, contribution of which to total NACs were increased by 10% and 5%, respectively. Positive matrix factorization analysis of combining LC-MS and AMS dataset was performed to identify the primary and secondary sources of NACs. Primary sources, e.g., traffic and solid-fuel combustion, accounted for 71% of the sum of 4-nitrophenol, 2,6-dimethyl-4-nitrophenol and 3-nitrosalicylic acid, suggesting important contribution of primary emissions to these NACs. The contribution of secondary sources, associated with two oxygenated organic aerosols, could contribute 66% to 4-nitrophenol, reflecting the link of such nitrated aromatic compounds to secondary organic aerosol source. Together with optical measurements, 4-nitrophenol presented a high contribution (>50%) to the identified BrC absorbance in the light range 250 and 550 nm was observed. This could highlight an important role of such NACs in ambient BrC light absorption, despite its mass contribution to total organic carbon was negligible. Our work could improve the understanding of the links between optical properties and chemical composition of BrC, and the difference between BrC chromophores from nonfoggy days and foggy days under the typical polluted atmospheric conditions.

1. Introduction

Light-absorbing organic aerosol (OA) – well-known as brown carbon (BrC) – has strong absorption of solar radiation, making important impact on the balance of atmospheric radiation and subsequent climate change (Alexander et al., 2008; Saleh, 2020). It can also have a significant impact on atmospheric chemical reactions by affecting the formation of ozone and other free radicals (e.g., OH and HO_2) (Wu et al., 2019). Ambient BrC is often attributed to a complex mixture of organic compounds, which presents strong wavelength dependence from the visible light region to the ultraviolet light region (Laskin et al., 2015). Different molecular composition of BrC could be generated from various sources, including primary emissions and secondary formation, which generally present different optical properties (Laskin et al., 2015; Moschos et al., 2018; Wang et al., 2019; Xu et al., 2022; Yan et al., 2015a; Zhang et al., 2020a). Very limited understanding in the sources and optical properties of BrC molecular composition has been making a large uncertainty of accurately assessing such impact of BrC on climate

* Corresponding authors.
** Corresponding authors.
E-mail addresses: caxinra@163.com (X. Ge), yjzhang@nuist.edu.cn (Y. Zhang).

https://doi.org/10.1016/j.envres.2022.113255
Received 5 March 2022; Received in revised form 31 March 2022; Accepted 3 April 2022
Available online 14 April 2022
0013-9351/

radiative forcing (IPCC, 2013). Therefore, it is critical to systematically investigate chemistry-source-optical properties of BrC at molecular composition levels.

High molecular weight compounds, such as humic-like substances (HULIS) (Voliotis et al., 2017), nitrated aromatic compounds (NACs) (Desyaterik et al., 2013), polycyclic aromatic hydrocarbons (PAHs) (Samburova et al., 2016), amorphous carbon spheres in biomass combustion (Hoffer et al., 2016), of BrC were often observed from ambient air. NACs, one of the important components of brown carbon, have been attracting extensive attention of relevant scholars (Desyaterik et al., 2013; Teich et al., 2017; Zhang et al., 2013). Previous studies have shown that nitrated aromatic compounds have a certain contribution to the BrC light absorption (Desyaterik et al., 2013; Zhang et al., 2013). The light absorption contribution of 16 nitrated aromatic compounds in fog aqueous solution accounted for 20%–55% of BrC in the wavelength range of 300–450 nm, most of which were nitrophenols (Desyaterik et al., 2013). Although the absolute mass of NACs in organic aerosols could be relatively low (Wang et al., 2018), its absorption contribution might not be ignored due to its strong absorption capacity per unit mass (Teich et al., 2017). However, we still do not have a good understanding of the chemical characteristics, sources and light absorption characteristics of nitrated aromatic compounds. Especially, the sources and optical properties of particulate NACs under foggy and/or polluted environments with substantial influence from intensive anthropogenic emissions remain unclear.

Some field observation and laboratory studies have found that the sources of NACs could be from primary emission and secondary formation (Harrison et al., 2005; Yan et al., 2015b). Some observations have confirmed that vehicle exhaust contains a certain amount of nitrophenols and nitrocatechols (Tremp et al., 1993). Recently, several studies reported that secondary formation could be an important source for NACs in BrC, and that its contribution might be more than one-third of total NACs (Harrison et al., 2005; Xu and Wang, 2013). The main secondary generation pathway is the nitration of phenol (or benzene) and its derivatives, which can be carried out in both gas phase and liquid phase (Harrison et al., 2005). Although different kinds of NACs sources were reported, it's still a huge challenge to quantify various sources of NACs due to limited measurement and analysis techniques.

In the past two decades, the widespread use of aerodyne aerosol mass spectrometer (AMS) has greatly promoted the chemical characterization and source analysis of OA (Daellenbach et al., 2020, 2015; Jimenez et al., 2009; Zhang et al., 2020b). Some recent studies have applied such AMS techniques coupled with multi-wavelength optical instruments to characterize the interaction between the optical properties, chemical composition and sources of ambient BrC (Chen et al., 2018, 2020; Lambe et al., 2013; Moschos et al., 2018). Especially, offline AMS technology has been developed to characterize environmental aerosol filter samples (Ge et al., 2017; Huang et al., 2014; Xu et al., 2015), cloud water (Kim et al., 2019), aqueous phase samples (Smith et al., 2014), etc. Despite AMS has one of the advantages for source apportionment of organic aerosol, it cannot provide molecular information of samples due to limited use of its detection system (Canagaratna et al., 2007; Jayne et al., 2000). Recently, some studies have tried to combine the data measured by AMS (i.e., mass spectra data) and molecular-level instruments to further identify and quantify sources of ambient organic aerosols with more detailed molecular information (Srivastava et al., 2019). This combining methodology could provide an effective way to analyze sources of ambient particulate matter at molecular levels (e.g., NACs).

The Yangtze River Delta (YRD) is one of the most prominent areas of air pollution in China, because of strong anthropogenic emissions (Zheng et al., 2018). In winter, the YRD region frequently suffers from haze air pollution with high humidity weather conditions. Previous studies have reported that fog and/or aqueous processing leads to enhanced secondary organic aerosol formation and evolution (Kaul et al., 2011). It is hypothesized that aqueous-phase chemistry in fog drops is responsible for increasing secondary organic aerosol (SOA) production, which could be also linked to secondary brown carbon formation via aqueous chemistry (Gilardoni et al., 2016; Wang et al., 2021). In this study, we conducted a field campaign during wintertime in Nanjing, a typical megacity in the YRD region. Off-line measurements including AMS and LC-MS, as well as optical instruments, and subsequent analysis were performed to quantify concentrations, sources, and light absorption characteristics of NACs in BrC. To explore impact of fog and/or aqueous processing on potential secondary NACs production, we did a comparison between polluted foggy and nonfoggy days.

2. Material and methods

2.1. Field observations

The sampling site was located at the campus of Nanjing University of Information Science and Technology (32.20 °N, 118.71 °E), surrounded by residential areas, main traffic roads and industrial areas. Atmospheric particulate matter samples were collected by a $PM_{2.5}$ large volume sampler (KB-1000, Jinshida, China) with a sample flow velocity of 1.05 m^3 min^{-1}. Around one-year sampling periods included 14 typical foggy and 12 nonfoggy days from December 2017 to December 2018. The sampling time in foggy days was set up into three-time intervals: (P1) 10:00–14:00, (P2) 14:00–18:00, (P3)18:00–9:00 next day, while 24 h time resolution was performed for collecting samples during nonfoggy days. Finally, total 54 $p.m._{2.5}$ samples were collected. Meteorological parameters, such as air temperature, relative humidity, wind speed, wind direction and precipitation, were simultaneously observed at the same sampling site.

2.2. Chemical analysis

To measure the NACs, including 3-methyl-4-nitrophenol (3M4NP), 2-methoxy-5-nitrophenol (2M5NP), 3-nitrosalicylic acid (3NSA), 2-methyl-4-nitrophenol (2M4NP), 2,6-dimethyl-4-nitrophenol (2,6D4NP), 4-nitroguaiacol (4NG), 4-nitrophenol (4NP), 4-nitrocatechol (4NC), the small piece samples with a diameter of 25 mm were first taken from the collected four quartz membranes samples by using ceramic scissors. The 350 ng of an internal standard solution (i.e., 4-nitrophenol-2, 3, 5, 6-d_4) was prepared for internal calibration. The 10 mL methanol was used to extract an aliquot of the filter thrice under ultrasonication. Pure nitrogen was used to concentrate and dry the extracts, which were later completely dissolved the remaining particles in the test tube using 500 μL of methanol followed by liquid chromatography/mass spectroscopy analysis (LC-MS, USA). The uncertainty caused by the volatilization of NACs during nitrogen drying will be further explored in the future. The more detailed description of the LC-MS can be found in previous literatures (Kitanovski et al., 2012a, 2012b).

Atlantis T3 C18 chromatographic column (2.1 mm × 150 mm, 3 m aperture, USA) was used to carry out the LC separation. The mobile phase used in the analysis was two phases, including phase C and phase D. The phase C was methanol containing 0.1% acetic acid, while the phase D was ultrapure water containing 0.1% acetic acid. The gradient separation was conducted with 0.1% acetic acid (v/v) in methanol (eluent C). The concentration of eluent C was 1% for the first 2.7 min, increased to 54% from 2.7 to 15.2 min, held at 54% for 1 min, and then increased to 90% from 16.2 to 32.7 min, held at 90% for 0.2 min. Finally, it decreased back to 1% from 32.9 to 34.7 min, held at 1% for 17.3 min.

The sample injection volume and the instrument flow rate were set to 10 μL and 0.19 mL/min, respectively. The column temperature was maintained at 45 °C. In this study, only ion currents with a specific mass-to-charge ratio (m/z) were detected, thereby improving the resolution of detection. In the process of sample detection analysis, a total of 9 nitrated aromatic compounds were determined according to the obtained mass spectra and retention time. The retention time of 9 kinds of

nitrated aromatic compounds is between 18.4 and 25.6 min. The setting of the mass spectrometer conditions was optimized for the parameters of each standard product through the mass spectrometer interface, including the deflection voltage of the precursor ion, the collision energy of the fragment ions, etc. A complete injection method is formed by setting the liquid phase conditions and mass spectrometry conditions as mentioned above.

2.3. UV–Vis light absorption analysis

Four round pieces of each filter (diameter: 20 mm) was extracted with 40 mL ultrapure water, and sonicated for 30 min. Then the insoluble species in water were removed through the 0.45 μm syringe filters, and we obtained the solution to be tested.

A UV–Vis spectrophotometer (UV-3600, Shimadzu, Japan) was used to measure the light absorption spectra of filter extracts at wavelengths of 250–800 nm. The light absorption coefficient at a certain wavelength of λ ($b_{abs,\lambda}$, M/m) can be calculated by using eq. (1) (Hecobian et al., 2010):

$$b_{abs,\lambda} = (A_\lambda - A_{700})\frac{V_l}{V_a \cdot l}\ln(10) \quad (1)$$

where A_{700} is used as a background value. V_l and V_a are the volumes of solvent (ultrapure water) and sampled air, respectively. L is the optical path length of the instrument (1 cm).

The dependence of light absorption characteristics of atmospheric brown carbon on wavelength is expressed by absorption Ångström exponent (AAE), and it is calculated by eq. (2) (Xie et al., 2020b):

$$b_{abs,\lambda} = K \cdot \lambda^{-AAE} \quad (2)$$

where K is a constant and the wavelength range is 300–600 nm.

In order to compare the difference of light absorption capacity between different samples, the mass absorption efficiency is introduced. The mass absorption efficiency (MAE, m^2/g) at 365 nm is calculated by eq. (3) (Huang et al., 2018):

$$MAE_{365} = \frac{b_{abs,365}}{WSOC} \quad (3)$$

where WSOC represents the concentration of water-soluble organic carbon (WSOC).

2.4. Offline AMS measurements and data analysis

In order to obtain high resolution organic aerosol mass spectra, the $PM_{2.5}$ filter samples were detected by offline AMS techniques (Daellenbach et al., 2015; Ge et al., 2017; Ye et al., 2017). In this study, an aerodyne soot particle aerosol mass spectrometry (SP-AMS) by setting the standard vaporizer mode was applied. More detailed description about SP-AMS can be found from previous studies (Onasch et al., 2012, 2016; Wang et al., 2020; Zhang et al., 2020b). For each sample, 4 circular filter membranes with a diameter of 20 mm were extracted in 20 mL ultrapure water. The uncertainty caused by different solvent extraction will be further explored in the future. The liquid extracts were aerosolized using an atomizer (TSI, Model 3076) and the mist passed through a silica-gel diffusion dryer to dry the particles which were subsequently analyzed by the SP-AMS.

The water-soluble organic matter (WSOM) was measured using offline SP-AMS, as detailed in Ge et al. (2017). Briefly, the aqueous extracts were nebulized using a constant output atomizer, dehumidified by a diffusion dryer filled with silica-gel, and then were sent to the SP-AMS. The SP-AMS data was processed using the Igor-based software toolkit SQUIRREL (version 1.56D) and PIKA (version 1.15D). The SP-AMS OA spectral data was combined with the NACs data to make a combined OA-NACs matrix dataset for the input data of positive matrix factorization (PMF) model. For the SP-AMS matrix data, the *m/z* range was from *m/z* 10 to *m/z* 185. More detailed information of PMF analysis can be found in many previous studies (Sun et al., 2012; Zhang et al., 2011). The uncertainty (unc) is estimated by equation according to the NAC concentration (c) and method detection limit (MDL), where the error fraction of 0.2 was taken. The uncertainty is calculated by eq. (4):

$$\text{unc} = \sqrt{(\text{Error Fraction} \times \text{c})^2 + +(0.5 \times MDL)^2} \quad (4)$$

3. Results and discussion

3.1. Concentration and variations

Fig. 1 shows time series of the mass concentration of NACs, WSOC, and water-insoluble organic carbon (WIOC) during the entire observation period. The NACs has a similar trend with WSOC, indicating that major NACs might closely related to WSOC and may come from similar sources. The average concentration of the total NACs mass ranged from 3.02 to 249.13 ng/m^3 with an average value of 105.20 ± 59.71 ng/m^3 for the foggy days, which is ~105.31% higher than that observed during nonfoggy days. The average concentration of the total NACs was 51.24 ± 33.32 ng/m^3 and 105.21 ± 59.70 ng/m^3 in nonfoggy days and foggy days, respectively (Table 1). The average concentration of the total NACs during foggy days in this study was obviously higher than those observed during wintertime in other cities in eastern China, such as Beijing (74 ± 51 ng/m^3) (Xla et al., 2020) and Jinan (48 ± 26 ng/m^3) (Wang et al., 2018). However, the average concentration in nonfoggy days was comparable to the results observed in the two cities. The mass concentration of WSOC (13.97 ± 6.78 μg/m^3) was generally higher than that of WIOC (6.52 ± 3.07 μg/m^3) during foggy days, suggesting a more important role of WSOC in contributing to organics in $PM_{2.5}$. The average concentration of WSOC in foggy days (16.10 ± 5.77 μg/m^3) was approximately 2.5 times higher than that in nonfoggy days (6.53 ± 4.39 μg/m^3), while limited difference of WIOC was observed between foggy days (6.76 ± 2.96 μg/m^3) and nonfoggy days (5.70 ± 3.40 μg/m^3). These results suggested that fog processing might pormote more WSOC formation rather than WIOC. One of the potential reasons could be enhanced secondary organic aerosol formation via aqueous chemistry under high humidity weater conditions and high fossil fuel combusition emission (Ervens et al., 2011; Tong et al., 2020; Wang et al., 2021; Ye et al., 2020; Yele et al., 2016). Additionally, adverse meteorological conditions, e.g., weak atmospheric diffusion, could make serious accmulation of air pollutants (Bei et al., 2016; Huang et al.; Wang et al., 2015), which might be another possible reason.

As shown in Fig. 1, the mass concentration of individual NACs shows very dynamic variations, likely due to changes of source emissions, secondary formation and meteorology. The 4NP was a dominate species in particulate NACs, with daily contribution ranging from 20% to 67%. As shown in Fig. 2, the relative contribution of the 2M4NP to the total NACs during foggy days (16%) was higher than that during nonfoggy days (6%). 3M4NP and 2,6D4NP were also consistent with 2M4NP. But the relative contribution of the 4NC to the total NACs during foggy days (13%) was lower than that during nonfoggy days (21%). During the entire study, NACs had a higher contribution to the total $PM_{2.5}$ mass, in comparison to the contribution from nitrosalicylic acid (NSA) oxidation compounds. This may be because there were many kinds of nitrophenol compounds measured in this study and their concentrations in the atmosphere were high. The contribution of NACs to the total $PM_{2.5}$ mass during nonfoggy and foggy days was 0.78 ± 0.71‰ and 0.53 ± 0.28‰, respectively. The concentration of the total NACs and its corresponding chemical compounds also showed distinct diel cycles during foggy days. For example, the concentration of the total NACs was generally the highest in the afternoon (0.75 ± 0.29‰), followed by the morning (0.55 ± 0.13‰) and evening (0.29 ± 0.16‰). From November 27 to December 3, 2018, the mass concentration of 4-nitrophenol and 4-nitrocatechol were also higher in the afternoon (43.63 and 19.41 ng/m^3) than

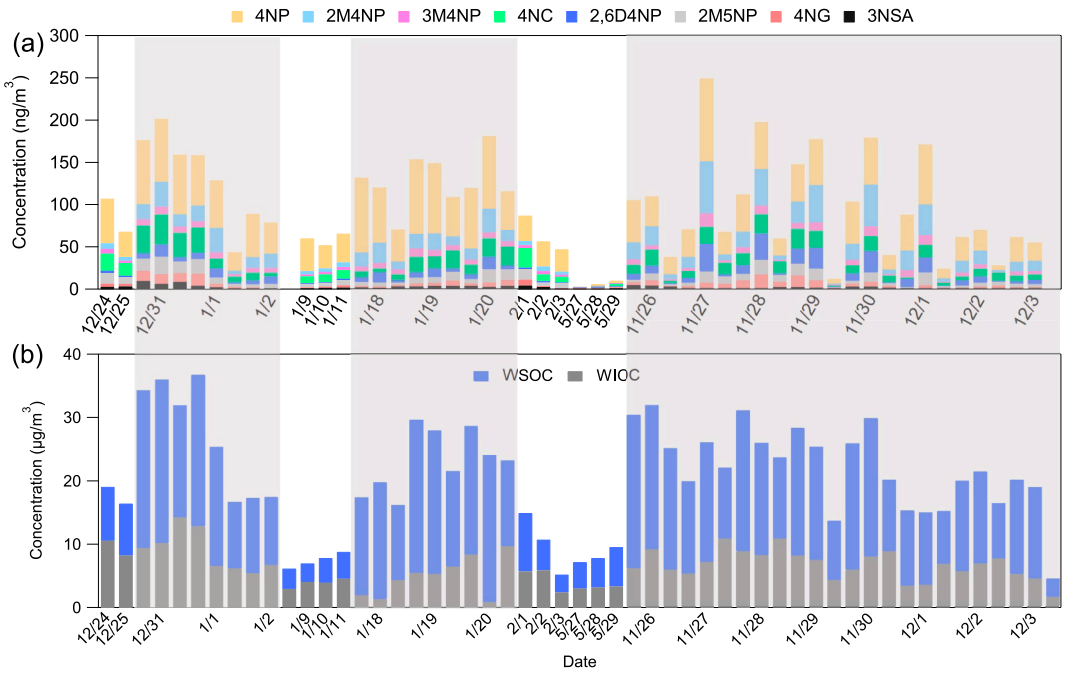

Fig. 1. Time series of (a) nitrated aromatic compounds and (b) water-soluble OC (WSOC) and water-insoluble OC (WIOC) during the entire campaign. Foggy days are marked as gray shaded areas.

Table 1
Mass concentration (ng/m^3) of NACs during nonfoggy and foggy days, respectively.

Compounds	Molecular weight	Non-foggy days	Foggy days
		Average	Average
4-nitrophenol	139.11	29.75 ± 22.41	45.44 ± 25.75
3-Methyl-4-nitrophenol	153.14	3.13 ± 3.06	5.84 ± 3.34
2-Methyl-4-nitrophenol	153.14	5.23 ± 5.92	17.93 ± 13.54
4-Nitrocatechol	155.11	23.83 ± 49.75	13.17 ± 9.05
2,6-Dimethyl-4-nitrophenol	167.16	1.76 ± 2.15	8.52 ± 8.03
2-Methoxy-5-nitrophenol	169.13	14 ± 29.92	7.3 ± 5.48
4-Nitroguaiacol	169.13	7.41 ± 18.71	4.77 ± 4.12
3-Nitrosalicylic acid	183.21	2.78 ± 3.47	2.24 ± 2.17
Total NACs		51.24 ± 33.32	105.21 ± 59.70

in the morning (40.65 and 10.72 ng/m^3) and evening (35.09 and 10.00 ng/m^3), respectively. This may be because the light was stronger and the photochemical reaction was better in the afternoon than that in other time periods. The daily concentrations changes of 2-methyl-4-nitrophenol and 3-methyl-4-nitrophenol were basically the same, and almost all of them were the highest in the second membrane sample taken in the afternoon, compared with the other two time periods.

The mass concentration of the total NACs presented good correlations with OC ($r = 0.73$) and WSOC ($r = 0.75$), respectively (see Fig. 3). These good correlations could not only validate reasonable variation trends for measured NACs, but it might also highlight that the observed NACs involved in similar atmospheric formation processes and/or sources. Especially, the good correlation between NACs and WSOC could also suggest that potential impact of aqueous process on the formation of major NACs. The sources and potential formation process will be further discussed in next section.

Table 2 presented the correlations between NACs and air pollutants. Overall, most NACs had good correlation (r = 0.29–0.57) with each other, indicating that they have the similar source and/or transformation pathway. The class of NPs compounds also had good correlations ($r = 0.29$–0.97) with each other. For example, 4NG and 4NC had overall good correlation with the NPs compounds. The correlation coefficient between 4NG and 4NC with 2M5NP was extremely high, which could explain that these three compounds were likely from the same

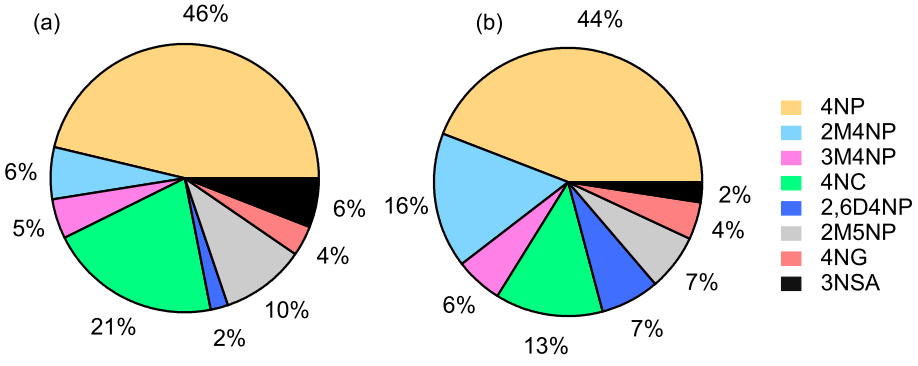

Fig. 2. Relative contribution of the nitrated aromatic compounds to the total NACs during (a) nonfoggy and (b) foggy days, respectively.

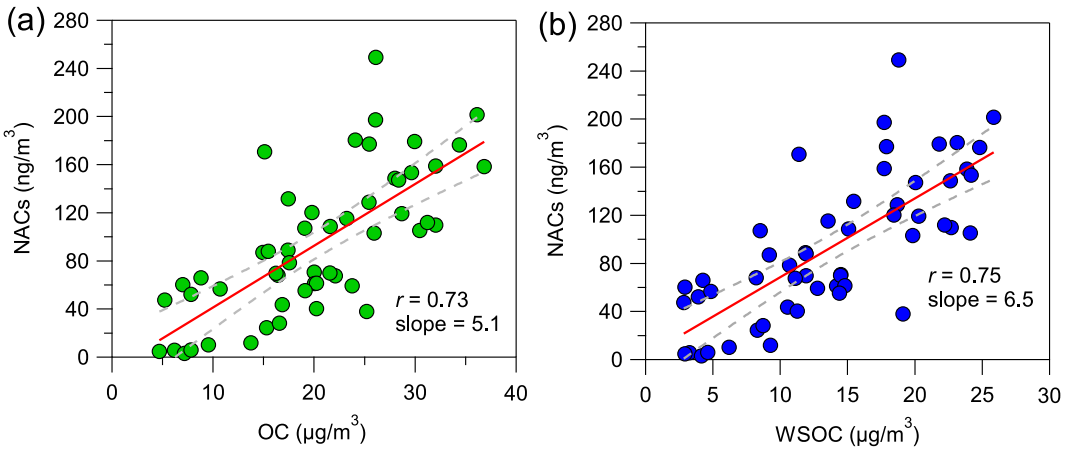

Fig. 3. Correlation between the total NACs with (a) OC and (b) WSOC, respectively.

Table 2
Pearson correlation coefficients between individual NAC species with aerosol chemical components and gas pollutants.

	3M4NP	2M5NP	3NSA	2M4NP	2,6D4NP	4NG	4NP	4NC	SO_2	NO_2	O_3
3M4NP	1	0.457[a]	0.337[a]	0.904[a]	0.827[a]	0.452[a]	0.858[a]	0.436[a]	0.340[b]	0.480[a]	0.042
2M5NP		1	0.708[a]	0.285[b]	0.231	0.979[a]	0.417[a]	0.993[a]	0.475[a]	0.488[a]	−0.026
3NSA			1	0.114	0.005	0.721[a]	0.469[a]	0.767[a]	0.389[a]	0.467[a]	−0.095
2M4NP				1	0.970[a]	0.300[b]	0.699[a]	0.245	0.249	0.474[a]	0.222
2,6D4NP					1	0.265	0.599[a]	0.181	0.239	0.457[a]	0.270
4NG						1	0.387[a]	0.979[a]	0.463[a]	0.573[a]	−0.036
4NP							1	0.414[a]	0287[b]	0.321[b]	0.011
4NC								1	0.463[a]	0.508[a]	−0.071
SO_2									1	0.311[b]	0.24
NO_2										1	−0.344[b]
O_3											1

[a] Significant correlation at the 0.01 level.
[b] Significant correlation at the 0.05 level.

source. 3NSA showed a better correlation with 4NC rather than with the MNPs compounds. This could suggest similar source of 3NSA and 4NC, but they might be different from the class NPs compounds. In the urban atmosphere, SO_2 is the particulate sulfate precursor mainly originated from coal combustion emission. The good correlation between SO_2 and some of NACs (e.g., 4NG and 4NC) may suggest one of possible NACs sources linked to coal combustion emission. In addition, some of NACs also had good correlations with NO_2, implying possible contribution of traffic emissions to NACs in this study. Further analysis in the sources of NACs will be further discussed in next section.

3.2. Source apportionment of NACs

Fig. 4 presents PMF-resolved mass spectra of OA-NACs sources. Time series of PMF-OA factors during the entire study could be found in Fig. 5. The mass spectrum of HOA is dominated by long-chain alkanes, such as $C_xH_y^+$ (62.0%), in which the O/C value is low (0.17). This factor could be representing for fresh traffic emissions, which is also consistent with many previous studies observed in urban environment (Zhang et al., 2011; Zhou et al., 2020). Meanwhile, 4NP, 2M4NP, 3M4NP and 2, 6D4NP made a relatively high contribution (4.76–48.08%) in the HOA factor profile. This results were in consistent with previous studies, where they found that these NACs are the main NACs emitted from vehicle exhaust (Lu et al., 2019a). On average, this HOA contributed 17.9% and 10.2% to the total OA-NACs during foggy and nonfoggy days, respectively (Fig. 6). The correlation between *m/z* 60 and *m/z* 73 tracer fragments $C_2H_4O_2^+$, $C_3H_5O_2^+$ ($r^2 = 0.47$ and 0.57) observed for the BBOA factor. In the factor profile, those m/z tracers and 4NC had the highest contribution. Meanwhile, some literature have showed that biomass burning (Li et al., 2020a) could also be a major source of ambient particulate 4NC. On average, this BBOA contributed 14.6% and 49.0% to the total OA-NACs during foggy and nonfoggy days, respectively (Fig. 6). The combustion activity of natural substances in nonfoggy days was more intense than that in foggy days, which may be because relatively sufficient light in nonfoggy days is conducive to the occurrence of photochemical reactions. For local OA, it is actually a POA with an oxygen carbon ratio of 0.44 in this study. The mass spectrum characteristics of this factor were similar to other POA tracer fragments, with the good correlations (r^2) with $C_4H_7^+$ (0.52), $C_4H_9^+$ (0.55), $C_3H_3O^+$ (0.56), $C_3H_5O^+$ (0.48), respectively. Among the NACs, 4NP, 2M4NP and 3M4NP made a high contribution in this factor profile (Fig. 4). These NACs are often associated with coal combustion emissions (Lu et al., 2019b). 4NP has been found related to industrial sector emissions (Lu et al., 2019a, 2021). Therefore, this local OA factor was likely an OA in the background of a northern suburb city. On average, this local OA contributed 30.6% and 2.8% to the total OA-NACs during foggy and nonfoggy days, respectively (Fig. 6). The contribution of foggy days was more obvious, which may be because the meteorological conditions of high humidity and low temperature in foggy days were more unfavorable to the diffusion of pollutants.

Compared with other factors, LO-OOA had the best correlation with nitrate. The O/C of this factor was 0.56, which higher and lower than primary factors and MO-OOA, respectively. Compared with MO-OOA, LO-OOA had a higher peak at *m/z* 29 and *m/z* 43. The high contribution of $C_xH_yO^+$ in the LO-OOA mass spectrum was also observed. In addition, 4NP was contained within the mass spectrum of LO-OOA, indicating a possible source of 4NP linked to this SOA factor. Such link could be due to that the 4NP has semi-volatility property (Pereira et al., 2014), which is comparable with the LO-OOA factor (Jimenez et al., 2009; Sun et al., 2018; Xu et al., 2017). Some previous studies

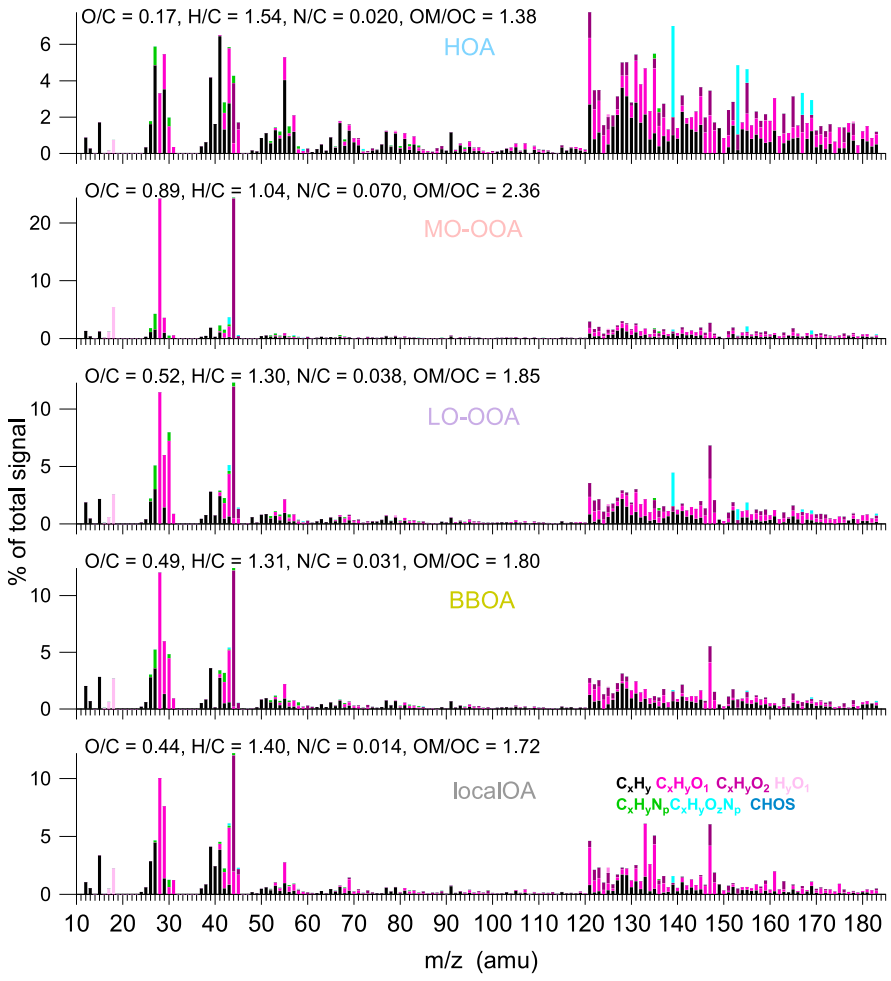

Fig. 4. Mass spectra of PMF OA factors, including HOA, BBOA, LO-OOA, MO-OOA, and local OA.

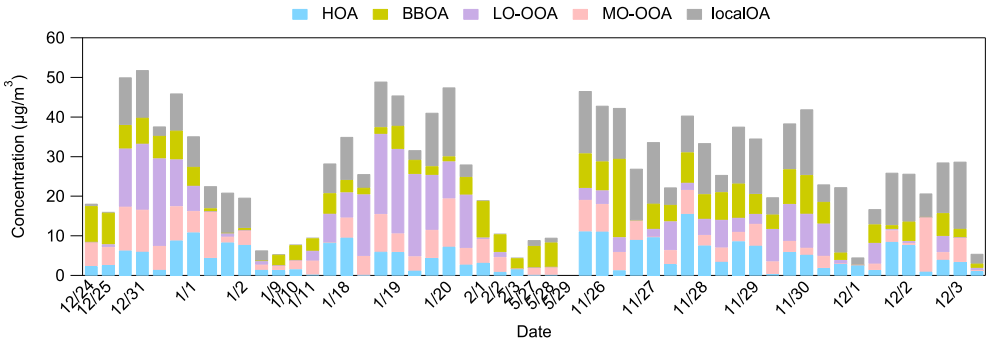

Fig. 5. Time series of PMF OA factors during the entire campaign.

have found that 3NSA in ambient particles could come from secondary formation and had substantial contribution to NACs (Li et al., 2020a). In the MO-OOA mass spectrum, *m/z* 44 and *m/z* 28 presented the highest contribution, which was consistent with the contribution of f_{CO} and f_{CO2} fragments. Meanwhile, the O/C value of this factor was 0.89, suggesting the more aged SOA factor observed in this study. The NACs in this factor were mainly 4NC and 2M5NP or 4NG (Fig. 7), which can be formed by secondary reaction (Li et al., 2020b). Therefore, this could further support the secondary characteristics of these NACs involved in MO-OOA factor.

As shown in Fig. 6a–d, the contribution of different OA factors to the total OA mass concentration and the total NACs mass concentration was different. Although BBOA contributed nearly half of the total OA mass concentration in nonfoggy days, its contribution to NACs was much less important (12.5%). This indicated that biomass burning produced more substances other than NACs. In comparison, traffic emissions in foggy days only accounted for 17.9% of the total OA mass concentration, yet it was the most significant contributor of the total NACs mass concentration (53.8%). This may be because NACs dominated the air pollutants emitted by traffic in foggy days. The contribution of traffic emissions to the concentration of NACs in foggy days was the highest, followed by the secondary source factors. During nonfoggy days, the contribution of

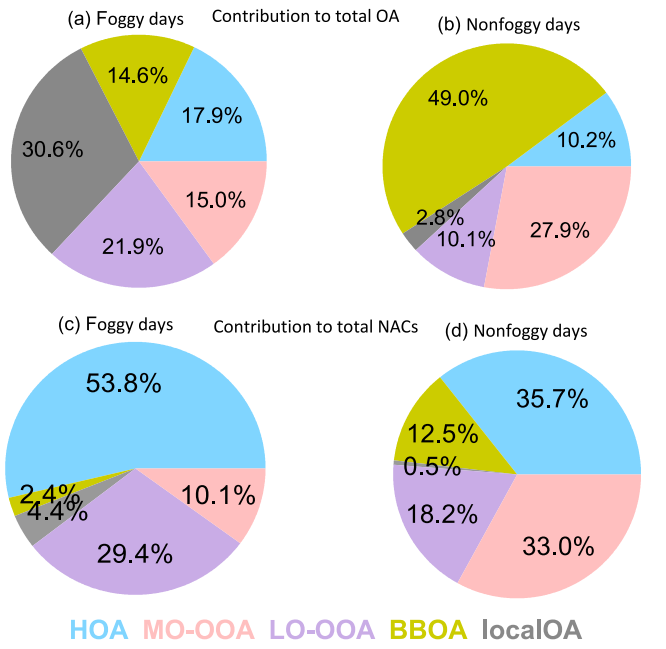

Fig. 6. Relative contribution of the OA factors to the total OA mass concentration (a and b) and (c and d) the total NACs mass concentration during (a and c) foggy and (b and d) nonfoggy days, respectively.

secondary aerosols to NACs was higher than traffic emissions.

As shown in Fig. 7, 4NP contributed to approximately 99% of NACs in local OA, both during foggy and nonfoggy days. For the two primary sources (i.e., HOA and BBOA) and a less oxidized SOA factor (i.e., LO-OOA), the contribution of 3M4NP or 2M4NP in foggy days was higher than that in nonfoggy days. In contrast, 4NC presented higher contribution during nonfoggy days than that during foggy days. This was probably because the contribution of traffic emissions was greater than that of biomass burning during foggy days (see Fig. 6). The 4NC and 2M5NP or 4NG observed in the MO-OOA factor dominated total mass concentration of these NACs during the entire periods, highlighting that these NACs were likely involved in secondary formation processes, such as photochemical and/or aqueous reactions.

3.3. Optical properties of NACs

The light absorption of the water extracts was mainly measured in the short wavelength range and decreased dramatically with the increase of wavelength. This is actually a typical feature of BrC (Li et al., 2019). Fig. S1 illustrated the average light absorption coefficient (b_{abs}) of water-soluble extracts at wavelengths (λ) from 300 to 600 nm. During the sampling period, the average Abs of the water extract of the aerosol samples at 365 nm was 16.91 ± 7.47 M/m (Fig. S1), which was much larger than that of the central Los Angeles (1.97 ± 0.93 M/m) (Soleimanian et al., 2020) and the northern suburbs of Nanjing (7.45 ± 3.73 M/m) (Xie et al., 2020a). The average b_{abs} during foggy days (16.91 M/m) was twice higher than that during nonfoggy days (7.41 M/m). The absorption Ångström exponent (AAE) can represent the wavelength dependence of the light absorption of BrC (Xie et al., 2020a). The difference in the AAE values of the water extract may be related to the difference in the chemical composition of the chromophore that only dissolves in water and is dominated by the main chemical substances (Sun et al., 2021; Xie et al., 2020a). In general, the AAE value of BrC in the atmosphere is closely related to its chemical composition and aerosol aging state (Bones et al., 2010; Chen and Bond, 2009). The AAE values in this study ranged from 7.26 to 7.67, with an average value of 7.46, as shown in Fig. S1. This value was higher than that in the northern suburbs of Nanjing (5.79) (Xie et al., 2020a), but less than that in the Central Los Angeles (8.71 ± 0.92) (Soleimanian et al., 2020).

The mass absorption efficiency of BrC at 365 nm (MAE_{365}) can characterize the difference of light absorption capacity between different samples (Xie et al., 2020a). The average value of MAE_{365} obtained in this study was 1.07 ± 0.27 m^2/g (Fig. S2). The value of MAE_{365} in this study was greater than that of Los Angeles (0.61 ± 0.22 m^2/g) (Soleimanian et al., 2020) and the northern suburbs of Nanjing (0.87 ± 0.29 m^2/g) (Xie et al., 2020a). The MAE_{365} between nonfoggy and foggy days was 1.12 and 1.06 m^2/g, respectively. We quantified a strong spectral dependence of absorption by BrC in the UV and diminished ultraviolet B radiation reaching the surface. Functionalized aromatic compounds were noteworthy chromophores responsible for the absorption of light by BrC (Li et al., 2020b). The absorption coefficients of standard NACs increased gradually with the increase of wavelength, and then decreased gradually after reaching a certain value (see Fig. 8a). The b_{abs} patterns for NACs was obviously different, where the b_{abs} of 4NP was the largest among the eight compounds. The maximum b_{abs} of 4NP and its methyl derivatives were generally higher than any of 4NG, 4NC and 3NSA, respectively. It is worth noting that the mass concentrations of the NACs only accounted for 0.078% and 0.053% of the total $PM_{2.5}$ during nonfoggy and foggy days, respectively. While the ratio of the absorption for the NACs to the total BrC absorption reached a maximum at approximately 330 nm with the value of 9.0% during non-foggy days and 4.45% during foggy days, respectively (Fig. 8b). Among them, 4NP was the most important BrC chromophores, followed by 4NC during nonfoggy days and 2M4NP during foggy days (Fig. 9). Meanwhile, the relevant parameters of eight NACs were listed in Table 3, such us

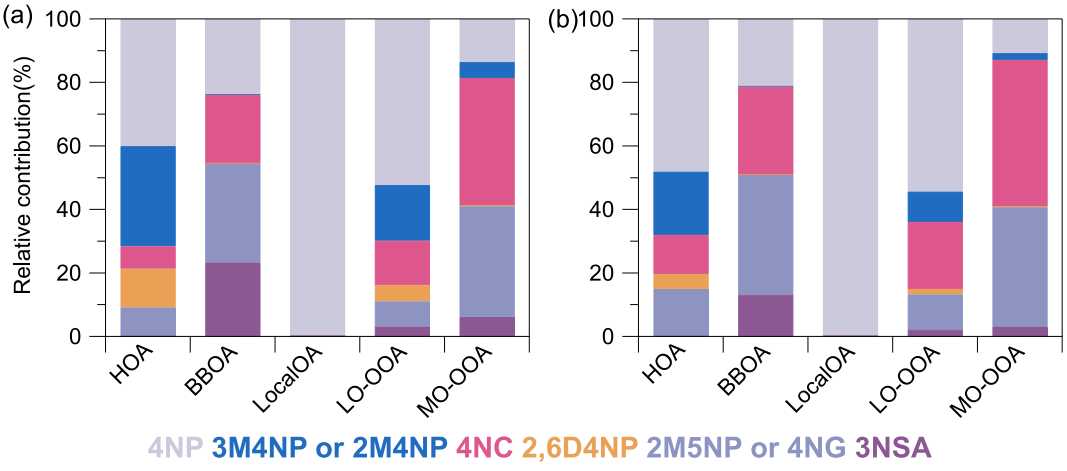

Fig. 7. Relative contribution of OA factors to different NACs during (a) foggy and (b) nonfoggy days, respectively.

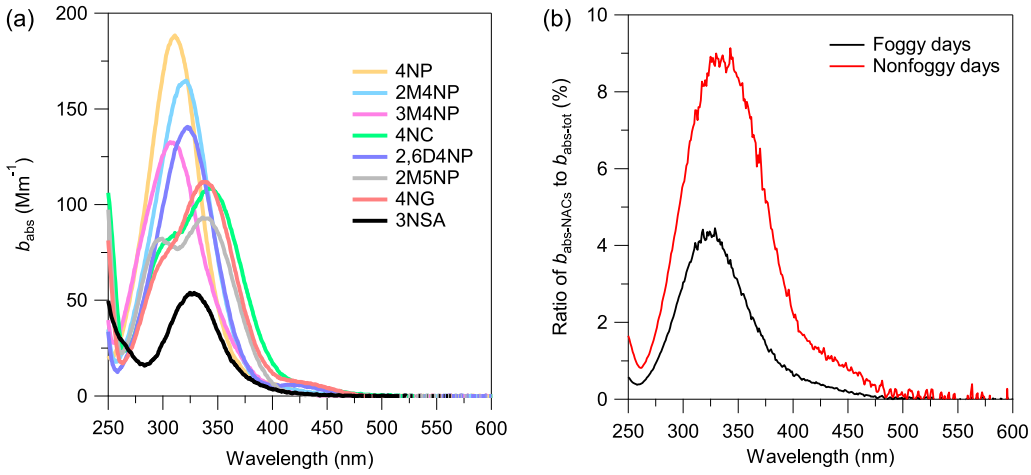

Fig. 8. Links between the optical properties and chemical compositions of BrC chromophores. (a) Absorption coefficient of standard NACs solutions (10 mg/l), and (b) Ratio of absorption coefficient of NACs to the total absorption among the wavelength of 250–600 nm.

formula, *m/z*, b_{abs} and MAE_{365}. The MAE_{365} values of some NACs obtained are consistent with previous studies (Xie et al., 2017).

4. Conclusions

Chemical composition, sources and optical properties of the eight NACs during winter foggy days in Nanjing were comprehensively characterized. The bulk concentration of NACs ranged from 3.02 to 249.13 ng/m^3, with an average value of 94.00 ng/m^3 during the entire study. The enhanced NACs concentration was evidently observed during foggy days, which was overall consistent with the WSOC variations. The 4NP was one of the most abundant compounds in NACs, with an average contribution of 46% during foggy days. PMF analysis of the combining the data measured by AMS and LC-MS identified five types of the NACs sources, which were corresponding to three primary (i.e., HOA, BBOA, and local OA) and two secondary OA sources (i.e., LO-OOA and MO-OOA). The largest contribution (54%) of the HOA factor, linked to urban traffic emissions, to the NACs mass was quantified during foggy days, followed by the OA factors of LO-OOA (29%) and MO-OOA (10%), etc. These results indicate important contribution of primary traffic emissions and secondary formation to the NACs observed during foggy days. Moreover, 4NP and 3M4NP or 2M4NP were mainly contributed from the HOA factor, while the large fraction of 4NC was found in the MO-OOA factor. However, further research would be required to further understand the formation mechanism of the secondary NACs factors in ambient air, especially under high humidity environment conditions. Optical measurements suggest that 4-nitrophenol dominated the measured BrC, accounting for 40%–60% of the concentration of identified chromophores. Meanwhile, 4-nitrophenol contributed more than 50% to the identified BrC absorbance in the wavelength range 250 and

Table 3
Absorption characteristics of standard nitrated aromatic compounds.

Compounds	Formula	*m/z*, [M-H]$^-$	b_{abs} (M/m)	MAE (m^2/g)
4-Nitrophenol	$C_6H_5NO_3$	138.16	20.49	2.05
2-Methyl-4-nitrophenol	$C_7H_7NO_3$	152.12	31.32	3.13
3-Methyl-4-nitrophenol	$C_7H_7NO_3$	152.18	26.71	2.67
4-Nitrocatechol	$C_6H_5NO_4$	154.01	81.51	8.15
2,6-Dimethyl-4-nitrophenol	$C_8H_9NO_3$	166.13	33.39	3.34
2-Methoxy-5-nitrophenol	$C_7H_7NO_4$	168.10	57.56	5.76
4-Nitroguaiacol	$C_7H_7NO_4$	168.09	67.93	6.79
3-Nitrosalicylic acid	$C_7H_5NO_5$	182.08	17.04	1.70

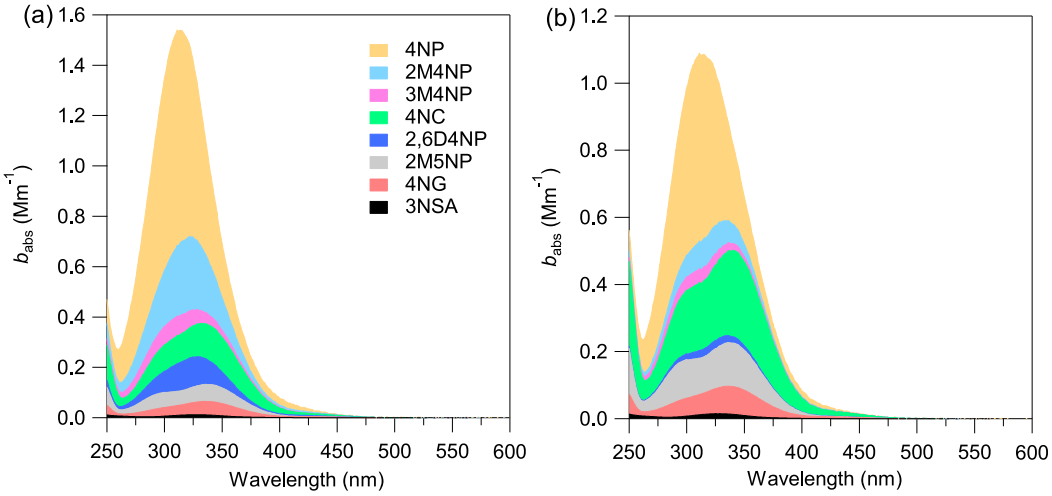

Fig. 9. Absorption coefficient of individual identified BrC chromophores (stacked area) linked to different NACs during (a) foggy days and (b) nonfoggy days, respectively.

550 nm. The ratio of the absorption for the NACs to the total BrC absorption reached at approximately 330 nm with the value of 4.5% during foggy days. These results suggest important contribution of NACs to aerosol light absorption at near UV wavelength during foggy days, although their contribution by mass was relatively low.

Author contributions

Chenjuan Gu: Data curation, Formal analysis, Investigation, Methodology, Validation, Software, Writing – original draft. **Shijie Cui**: Methodology, Software.**Xinlei Ge**: Conceptualization, Funding acquisition, Writing – review & editing, Supervision. **Zhiying WangMeijuan Chen**, **Zihe Qian**: Data curation. **Zhiyi LiuXinfeng Wang**: Methodology.**Yunjiang Zhang**: Conceptualization, Software, Writing – review & editing.

Declaration of competing interest

The authors declare that they have no known competing financial interests or personal relationships that could have appeared to influence the work reported in this paper.

Acknowledgements

This work was supported by the Natural Science Foundation of China (grant no. 21976093and grant no. 42021004).

Appendix A. Supplementary data

Supplementary data to this article can be found online at https://doi.org/10.1016/j.envres.2022.113255.

References

Alexander, D., et al., 2008. Brown carbon spheres in east asian outflow and their optical properties. Science 321, 833–836. https://doi.org/10.1126/science.1155296.

Bei, N., et al., 2016. Critical role of meteorological conditions in a persistent haze episode in the Guanzhong basin, China. Sci. Total Environ. 550, 273–284. https://doi.org/10.1016/j.scitotenv.2015.12.159.

Bones, D., et al., 2010. Appearance of strong absorbers and fluorophores in limonene-O3 secondary organic aerosol due to NH4+-mediated chemical aging over long time scales. J. Geophys. Res. 115 https://doi.org/10.1029/2009JD012864.

Canagaratna, M., et al., 2007. Chemical and microphysical characterization of ambient aerosols with the aerodyne aerosol mass spectrometer. Mass Spectrom. Rev. 26, 185–222. https://doi.org/10.1002/mas.20115.

Chen, Y., et al., 2020. Brown carbon in atmospheric fine particles in Yangzhou, China: light absorption properties and source apportionment. Atmos. Res. 244, 105028. https://doi.org/10.1016/j.atmosres.2020.105028.

Chen, Y., Bond, T.C., 2009. Light absorption by organic carbon from wood combustion. Atmos. Chem. Phys. 10, 1773–1787. https://doi.org/10.5194/acp-10-1773-2010.

Chen, Y., et al., 2018. Seasonal light absorption properties of water-soluble brown carbon in atmospheric fine particles in Nanjing, China. Atmos. Environ. 187, 230–240. https://doi.org/10.1016/j.atmosenv.2018.06.002.

Daellenbach, K., et al., 2015. Characterization and source apportionment of organic aerosol using offline aerosol mass spectrometry. Atmospheric Measurement Techniques Discussions. https://doi.org/10.5194/amtd-8-8599-2015.

Daellenbach, K., et al., 2020. Sources of particulate-matter air pollution and its oxidative potential in Europe. Nature 587, 414–419. https://doi.org/10.1038/s41586-020-2902-8.

Desyaterik, Y., et al., 2013. Speciation of "brown" carbon in cloud water impacted by agricultural biomass burning in eastern China. J. Geophys. Res. Atmos. 118, 7389–7399. https://doi.org/10.1002/jgrd.50561.

Ervens, B., et al., 2011. Secondary organic aerosol formation in cloud droplets and aqueous particles (aqSOA): a review of laboratory, field and model studies. Atmos. Chem. Phys. 11, 22301–22383. https://doi.org/10.5194/acp-11-11069-2011.

Ge, X., et al., 2017. Aerosol characteristics and sources in Yangzhou, China resolved by offline aerosol mass spectrometry and other techniques. Environ. Pollut. 225, 74. https://doi.org/10.1016/j.envpol.2017.03.044.

Gilardoni, S., et al., 2016. Direct observation of aqueous secondary organic aerosol from biomass-burning emissions. Proc. Natl. Acad. Sci. Unit. States Am. 113, 10013–10018. https://doi.org/10.1073/pnas.1602212113.

Harrison, M., et al., 2005. Evaluation of the pathways of tropospheric nitrophenol formation from benzene and phenol using a multiphase model. Atmos. Chem. Phys. 5, 1679–1695. https://doi.org/10.5194/acp-5-1679-2005.

Hecobian, A., et al., 2010. Water-Soluble Organic Aerosol material and the light-absorption characteristics of aqueous extracts measured over the Southeastern United States. Atmos. Chem. Phys. 10, 5965–5977. https://doi.org/10.5194/acp-10-5965-2010.

Hoffer, A., et al., 2016. Brown carbon absorption in the red and near infrared spectral region. Atmos. Chem. Phys. 1–16. https://doi.org/10.5194/acp-2016-452.

Huang, R., et al., 2018. Brown carbon aerosol in urban Xi'an, Northwest China: the composition and light absorption properties. Environ. Sci. Technol. 52, 6825–6833. https://doi.org/10.1021/acs.est.8b02386.

Huang, R., et al., 2014. High secondary aerosol contribution to particulate pollution during haze events in China Nature, 514, pp. 218–222. https://doi.org/10.1038/nature13774.

Huang, X., et al., 2020. Amplified transboundary transport of haze by aerosol–boundary layer interaction in China. Nat. Geosci. 13, 428–434. https://doi.org/10.1038/s41561-020-0583-4.

IPCC, 2013. Climate Change 2013: The Physical Science Basis. Contribution of Working Group I to the Fifth Assessment Report of the Intergovernmental Panel on Climate Change. Cambridge University Press, Cambridge, United Kingdom and New York, NY, USA.

Jayne, J., et al., 2000. Development of an aerosol mass spectrometer for size and composition analysis of submicron particles. Aerosol. Sci. Technol. 33, 49–70. https://doi.org/10.1080/027868200410840.

Jimenez, J., et al., 2009. Evolution of organic aerosols in the atmosphere. Science 326, 1525–1529. https://doi.org/10.1126/science.1180353.

Kaul, D., et al., 2011. Secondary organic aerosol: a comparison between foggy and nonfoggy days. Environ. Sci. Technol. 45, 7307–7313. https://doi.org/10.1021/es201081d.

Kim, H., et al., 2019. Chemical processing of water-soluble species and formation of secondary organic aerosol in fogs. Atmos. Environ. 200, 158–166. https://doi.org/10.1016/j.atmosenv.2018.11.062.

Kitanovski, Z., et al., 2012a. Development of a liquid chromatographic method based on ultraviolet-visible and electrospray ionization mass spectrometric detection for the identification of nitrocatechols and related tracers in biomass burning atmospheric organic aerosol. Rapid Commun. Mass Spectrom. 26, 793–804. https://doi.org/10.1002/rcm.6170.

Kitanovski, Z., et al., 2012b. Liquid chromatography tandem mass spectrometry method for characterization of monoaromatic nitro-compounds in atmospheric particulate matter. J. Chromatogr. A 1268, 35–43. https://doi.org/10.1016/j.chroma.2012.10.021.

Lambe, A., et al., 2013. Relationship between oxidation level and optical properties of secondary organic aerosol. Environ. Sci. Technol. 47, 6349–6357. https://doi.org/10.1021/es401043j.

Laskin, A., et al., 2015. Chemistry of atmospheric Brown carbon. Chem. Rev. 115, 4335. https://doi.org/10.1021/cr5006167.

Li, M., et al., 2020a. Nitrated phenols and the phenolic precursors in the atmosphere in urban Jinan, China. Sci. Total Environ. 714, 136760. https://doi.org/10.1016/j.scitotenv.2020.136760.

Li, X., et al., 2020b. Characterizing chemical composition and light absorption of nitroaromatic compounds in the winter of Beijing. Atmos. Environ. 237, 117712. https://doi.org/10.1016/j.atmosenv.2020.117712.

Li, Z., et al., 2019. Light absorption properties and potential sources of particulate brown carbon in the Pearl River Delta region of China. Atmos. Chem. Phys. 19, 11669–11685. https://doi.org/10.5194/acp-19-11669-2019.

Lu, C., et al., 2019a. Emissions of fine particulate nitrated phenols from various on-road vehicles in China. Environ. Res. 179, 108709. https://doi.org/10.1016/j.envres.2019.108709.

Lu, C., et al., 2019b. Emissions of fine particulate nitrated phenols from residential coal combustion in China. Atmos. Environ. 203, 10–17. https://doi.org/10.1016/j.atmosenv.2019.01.047.

Lu, C., et al., 2021. Substantial emissions of nitrated aromatic compounds in the particle and gas phases in the waste gases from eight industries. Environ. Pollut. 283, 117132. https://doi.org/10.1016/j.envpol.2021.117132.

Moschos, V., et al., 2018. Source apportionment of Brown carbon absorption by coupling ultraviolet-visible spectroscopy with aerosol mass spectrometry. Environ. Sci. Technol. Lett. 5, 302–308. https://doi.org/10.1021/acs.estlett.8b00118.

Onasch, T., et al., 2012. Soot particle aerosol mass spectrometer: development, validation, and initial application. Aerosol. Sci. Technol. 46, 804–817. https://doi.org/10.1080/02786826.2012.663948.

Onasch, T., et al., 2016. Observation of fullerene soot in eastern China. Environ. Sci. Technol. Lett. 3, 121–126. https://doi.org/10.1021/acs.estlett.6b00044.

Pereira, L., et al., 2014. Investigation of high Resolution Mass Spectrometry to Study the Formation and Evolution Ofsecondary Organic Aerosol. University of York. http://etheses.whiterose.ac.uk/8285/.

Saleh, R., 2020. From measurements to models: toward accurate representation of Brown carbon in climate calculations. Current Pollution Reports 6. https://doi.org/10.1007/s40726-020-00139-3.

Samburova, V., et al., 2016. Polycyclic aromatic hydrocarbons in biomass-burning emissions and their contribution to light absorption and aerosol toxicity. Sci. Total Environ. 568, 391–401. https://doi.org/10.1016/j.scitotenv.2016.06.026.

Smith, J., et al., 2014. Secondary organic aerosol production from aqueous reactions of atmospheric phenols with an organic triplet excited state. Environ. Sci. Technol. 48, 1049. https://doi.org/10.1021/es4045715.

Soleimanian, E., et al., 2020. Impact of secondary and primary particulate matter (PM) sources on the enhanced light absorption by brown carbon (BrC) particles in central Los Angeles. Sci. Total Environ. 705, 135902. https://doi.org/10.1016/j.scitotenv.2019.135902.

Srivastava, D., et al., 2019. Speciation of organic fractions does matter for aerosol source apportionment. Part 3: combining off-line and on-line measurements. Sci. Total Environ. 690, 944–955. https://doi.org/10.1016/j.scitotenv.2019.06.378.
Sun, H., et al., 2021. Molecular composition and optical property of humic-like substances (HULIS) in winter-time PM2.5 in the rural area of North China Plain. Atmos. Environ. 252, 118316. https://doi.org/10.1016/j.atmosenv.2021.118316.
Sun, Y., et al., 2018. Source apportionment of organic aerosol from 2-year highly time-resolved measurements by an aerosol chemical speciation monitor in Beijing, China. Atmos. Chem. Phys. 18, 8469–8489. https://doi.org/10.5194/acp-18-8469-2018.
Sun, Y., et al., 2012. Factor analysis of combined organic and inorganic aerosol mass spectra from high resolution aerosol mass spectrometer measurements. Atmos. Chem. Phys. 12, 8537–8551. https://doi.org/10.5194/acp-12-8537-2012.
Teich, M., et al., 2017. Contributions of nitrated aromatic compounds to the light absorption of water-soluble and particulate brown carbon in different atmospheric environments in Germany and China. Atmos. Chem. Phys. 17, 1653–1672. https://doi.org/10.5194/acp-2016-647.
Tong, Y., et al., 2020. Quantification of solid fuel combustion and aqueous chemistry contributions to secondary organic aerosol during wintertime haze events in Beijing. Atmos. Chem. Phys. 21, 9859–9886. https://doi.org/10.5194/acp-2020-835.
Tremp, J., et al., 1993. Phenols and nitrophenols as tropospheric pollutants: emissions from automobile exhausts and phase transfer in the atmosphere. Water Air Soil Pollut. 68, 113–123. https://doi.org/10.1007/BF00479396.
Voliotis, A., et al., 2017. New Insights on humic-like Substances Associated with Wintertime Urban Aerosols from Central and Southern Europe: Size-Resolved Chemical Characterization and Optical Properties. Atmospheric Environment. https://doi.org/10.1016/j.atmosenv.2017.07.024.
Wang, J., et al., 2020. Characterization of submicron organic particles in beijing during summertime: comparison between SP-AMS and HR-AMS. Atmos. Chem. Phys. 20, 14091–14102. https://doi.org/10.5194/acp-2020-750.
Wang, J., et al., 2021. Aqueous production of secondary organic aerosol from fossil-fuel emissions in winter Beijing haze. Proc. Natl. Acad. Sci. U. S. A 118, 8. https://doi.org/10.1073/pnas.2022179118.
Wang, L., et al., 2018. Observations of fine particulate nitrated phenols in four sites in northern China: concentrations, source apportionment, and secondary formation. Atmos. Chem. Phys. 18, 4349–4359. https://doi.org/10.5194/acp-18-4349-2018.
Wang, Q., et al., 2019. High contribution of secondary Brown carbon to aerosol light absorption in the southeastern margin of Tibetan plateau. Geophys. Res. Lett. 46, 4962–4970. https://doi.org/10.1029/2019GL082731.
Wang, S., et al., 2015. Atmospheric characteristics of a serious haze episode in Xi'an and the influence of meteorological conditions. Acta Sci. Circumstantiae 35, 3452–3462. https://doi.org/10.13671/j.hjkxxb.2015.0100.
Wu, G., et al., 2019. Water-soluble Brown carbon in atmospheric aerosols from godavari (Nepal), A regional representative of south asia. Environ. Sci. Technol. 53, 3471–3479. https://doi.org/10.1021/acs.est.9b00596.
Xie, M., et al., 2017. Light absorption of secondary organic aerosol: composition and contribution of nitroaromatic compounds. Environ. Sci. Technol. 51, 11607–11616. https://doi.org/10.1021/acs.est.7b03263.
Xie, X., et al., 2020a. Light-absorbing and fluorescent properties of atmospheric brown carbon: a case study in Nanjing, China. Chemosphere 251, 126350. https://doi.org/10.1016/j.chemosphere.2020.126350.
Xie, X., et al., 2020b. Light-absorbing and fluorescent properties of atmospheric brown carbon: a case study in Nanjing, China. Chemosphere 251, 126350. https://doi.org/10.1016/j.chemosphere.2020.126350.
Xla, B., et al., 2020. Light absorption properties of brown carbon (BrC) in autumn and winter in Beijing: composition, formation and contribution of nitrated aromatic compounds. Atmos. Environ. 223 https://doi.org/10.1016/j.atmosenv.2020.117289.
Xu, C., Wang, L., 2013. Atmospheric oxidation mechanism of phenol initiated by OH radical. J. Phys. Chem. 117, 2358–2364. https://doi.org/10.1021/jp308856b.
Xu, J., et al., 2022. Atmospheric Brown carbon on the Tibetan plateau: regional differences in chemical composition and light absorption properties. Environ. Sci. Technol. Lett. 9, 219–225. https://doi.org/10.1021/acs.estlett.2c00016.
Xu, J., et al., 2015. Chemical composition and size distribution of summertime PM2.5 at a high altitude remote location in the northeast of the Qinghai-Xizang (Tibet) Plateau: insights into aerosol sources and processing in free troposphere. Atmos. Chem. Phys. 15, 5069–5081. https://doi.org/10.5194/acp-15-5069-2015.
Xu, W., et al., 2017. Effects of aqueous-phase and photochemical processing on secondary organic aerosol formation and evolution in Beijing, China. Environ. Sci. Technol. 51, 762–770. https://doi.org/10.1021/acs.est.6b04498.
Yan, C., et al., 2015a. Chemical characteristics and light-absorbing property of water-soluble organic carbon in Beijing: biomass burning contributions. Atmos. Environ. 121, 4–12. https://doi.org/10.1016/j.atmosenv.2015.05.005.
Yan, L., et al., 2015b. Correlation between coal structure and release of the two organic compounds during pyrolysis. Fuel 145, 12–17. https://doi.org/10.1016/j.fuel.2014.12.056.
Ye, Z., et al., 2017. Chemical characterization of fine particulate matter in Changzhou, China, and source apportionment with offline aerosol mass spectrometry. Atmos. Chem. Phys. 17, 2573–2592. https://doi.org/10.5194/acp-17-2573-2017.
Ye, Z., et al., 2020. Aqueous-phase oxidation of three phenolic compounds by hydroxyl radical: insight into secondary organic aerosol formation yields, mechanisms, products and optical properties. Atmos. Environ. 223, 117240–117241. https://doi.org/10.1016/j.atmosenv.2019.117240, 117240.12.
Yele, S., et al., 2016. Primary and secondary aerosols in Beijing in winter: sources, variations andprocesses. Atmos. Chem. Phys. 16, 1–41. https://doi.org/10.5194/acp-16-8309-2016.
Zhang, Q., et al., 2011. Understanding atmospheric organic aerosols via factor analysis of aerosol mass spectrometry: a review. Anal. Bioanal. Chem. 401, 3045–3067. https://doi.org/10.1007/s00216-011-5355-y.
Zhang, X., et al., 2013. Sources, composition and absorption ngstrm exponent of light-absorbing organic components in aerosol extracts from the Los Angeles basin. Environ. Sci. Technol. 47, 3685–3693. https://doi.org/10.1021/es305047b.
Zhang, Y., et al., 2020a. Substantial brown carbon emissions from wintertime residential wood burning over France. Sci. Total Environ. 743, 140752. https://doi.org/10.1016/j.scitotenv.2020.140752.
Zhang, Y., et al., 2020b. Aerosol measurements by soot particle aerosol mass spectrometer: a review. Current Pollution Reports 6, 440–451. https://doi.org/10.1007/s40726-020-00162-4.
Zheng, B., et al., 2018. Trends in China's anthropogenic emissions since 2010 as the consequence of clean air actions. Atmos. Chem. Phys. 18, 14095–14111. https://doi.org/10.5194/acp-2018-374.
Zhou, W., et al., 2020. A review of aerosol chemistry in asia: insights from aerosol mass spectrometer measurements. Environmental Science: Processes Impacts. https://doi.org/10.1039/D0EM00212G.